FULL-LENGTH PAPER

THE PROTEIN SOCIETY WILEY

Ca²⁺ attenuates nucleation activity of leiomodin

Garry E. Smith Jr.[1] | Dmitri Tolkatchev[1] | Cristina Risi[2] |
Madison Little[1] | Carol C. Gregorio[3] | Vitold E. Galkin[2] | Alla S. Kostyukova[1]

[1]Voiland School of Chemical Engineering and Bioengineering, Washington State University, Pullman, Washington

[2]Department of Physiological Sciences, Eastern Virginia Medical School, Norfolk, Virginia

[3]Department of Cellular and Molecular Medicine and Sarver Molecular Cardiovascular Research Program, University of Arizona, Tucson, Arizona, USA

Correspondence
Alla S. Kostyukova, The Voiland School of Chemical Engineering & Bioengineering, Washington State University, Wegner Hall, Pullman, WA 99164, USA.
Email: alla.kostyukova@wsu.edu

Vitold E. Galkin, Department of Physiological Sciences, Eastern Virginia Medical School, Norfolk, VA 23507, USA.
Email: galkinve@evms.edu

Review Editor: John Kuriyan

Abstract

A transient increase in Ca²⁺ concentration in sarcomeres is essential for their proper function. Ca²⁺ drives striated muscle contraction via binding to the troponin complex of the thin filament to activate its interaction with the myosin thick filament. In addition to the troponin complex, the myosin essential light chain and myosin-binding protein C were also found to be Ca²⁺ sensitive. However, the effects of Ca²⁺ on the function of the tropomodulin family proteins involved in regulating thin filament formation have not yet been studied. Leiomodin, a member of the tropomodulin family, is an actin nucleator and thin filament elongator. Using pyrene-actin polymerization assay and transmission electron microscopy, we show that the actin nucleation activity of leiomodin is attenuated by Ca²⁺. Using circular dichroism and nuclear magnetic resonance spectroscopy, we demonstrate that the mostly disordered, negatively charged region of leiomodin located between its first two actin-binding sites binds Ca²⁺. We propose that Ca²⁺ binding to leiomodin results in the attenuation of its nucleation activity. Our data provide further evidence regarding the role of Ca²⁺ as an ultimate regulator of the ensemble of sarcomeric proteins essential for muscle function.

KEYWORDS

actin, circular dichroism, leiomodin, nuclear magnetic resonance, pyrene-actin polymerization, transmission electron microscopy

Summary Statement

Ca²⁺ fluctuations in striated muscle sarcomeres modulate contractile activity via binding to several distinct families of sarcomeric proteins. The effects of Ca²⁺ on the activity of leiomodin—an actin nucleator and thin filament length regulator—have remained unknown. In this study, we demonstrate that Ca²⁺ binds directly to leiomodin and attenuates its actin nucleating activity. Our data emphasizes the ultimate role of Ca²⁺ in the regulation of the sarcomeric protein interactions.

Garry E. Smith Jr., Dmitri Tolkatchev contributed equally to this study.

1 | INTRODUCTION

Striated muscle contraction is responsible for the beating of the heart and for muscle-based motility. The sarcomere is the most basic contractile unit of striated muscle. Two of the sarcomere's fundamental components are the overlapping thin and thick filaments, made primarily of actin and myosin, respectively. Periodic transient increases in Ca^{2+} levels in striated muscle cells regulate the function of integral muscle proteins, such as troponin, myosin, myosin-binding protein C, and titin.[1–5] Ca^{2+} drives striated muscle contraction via binding to the troponin complex of the thin filament to activate its interaction with the myosin thick filament. Interaction between the myosin essential light chain and Ca^{2+} activates the myosin holoenzyme.[5] Ca^{2+} restores the inhibitory capacity of phosphorylated myosin-binding protein C.[3] Ca^{2+} binding to the immunoglobulin domain of titin results in increased stability and stiffness.[1] Another essential sarcomeric protein with a potential to bind cations is leiomodin (Lmod), a protein of the actin-binding tropomodulin (Tmod) family. In particular, Lmod contains a long negatively charged region of unknown function (Figure 1)[6]; this region could potentially bind Ca^{2+}.

The process of building, maintaining, and repairing of the thin filament is complex and involves Lmod, and Tmod, along with ZASP, nebulin, formins, profilin, and CapZ, at various stages of development (for review, see[7]). Tmod family proteins, with affinity for both actin and tropomyosin (Tpm), have a critical role in controlling thin filament lengths.[8–12] Regulation of thin filament length is crucial to ensure an optimal overlap between thin and thick filaments and an optimal force generation during muscle contraction. Additionally, the ability of Lmod to nucleate actin was proposed to play a role in de novo formation of thin filaments.[13,14] Loss of Lmod causes aberrant sarcomere assembly and severe muscle dysfunction.[15–18] Yet, nothing is known about upstream regulation of Lmod function.

There are three Lmod isoforms, Lmod1, Lmod2, and Lmod3, each expressed primarily in smooth, cardiac, or skeletal muscle, respectively.[6,19] In this study, we sought to examine whether Ca^{2+} levels affect the nucleating activity of the cardiac isoform of Lmod, Lmod2. Lmod2 is a modular protein with a specific organization of Tpm- and actin-binding sites (Figure 1; for review see[6]). In order of their appearance in the sequence from the N-terminus, there is a Tpm-binding site (TpmBS1), an actin-binding site (ABS1), a leucine-rich repeat (LRR) domain serving as the second actin-binding site (ABS2), and a Wiskott-Aldrich Homology 2 (WH2) domain, serving as the third actin-binding site (ABS3). There are two disordered flexible linkers, the first one connecting ABS1 and ABS2 and the second one connecting ABS2 and ABS3 (Figure 1).

Using both pyrene-actin polymerization assay and transmission electron microscopy (TEM), we have found that Lmod2 nucleation activity is attenuated by Ca^{2+}. Using nuclear magnetic resonance (NMR), we have shown that Ca^{2+} binds to the linker between the first two actin-binding sites in Lmod2. We propose that Ca^{2+} binding to Lmod2 causes the observed decrease in Lmod2 nucleation activity. Lmod2 is the first pointed-end binding protein, whose function has been shown to be Ca^{2+}-sensitive.

2 | RESULTS

## 2.1 | Effect of Ca^{2+} on Lmod2-induced actin nucleation

To test whether Ca^{2+} has an effect on Lmod2-induced actin nucleation, we measured polymerization of pyrene-labeled G-actin in the presence and absence of Lmod2 at high (pCa = 3.7) or low (pCa = 9) levels of Ca^{2+} (Figure 2). Since the pyrene-labeled actin fluorescence is directly proportional to the extent of actin polymerization, the lag time and maximum polymerization rate can be deduced from the changes in fluorescence.

It was shown that Ca^{2+} negatively affects the rate of actin polymerization.[20] Therefore, to properly evaluate the effect of Lmod2, first, we established at which concentrations of G-actin the polymerization rates at pCa = 9 and pCa = 3.7 were similar. We compared the polymerization rate of 3 μM G-actin at pCa = 3.7 with
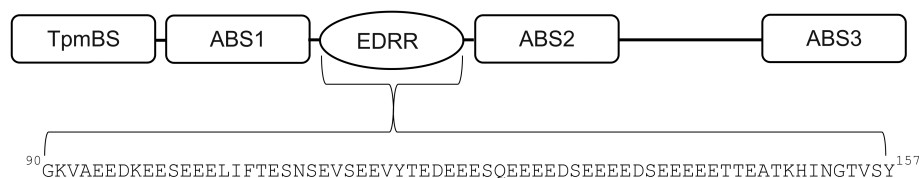
FIGURE 1 Domain structure of Lmod2. Lmod2 is comprised of several functionally distinguished regions: TpmBS – Tropomyosin-binding site, ABS – Actin-binding site, EDRR – Glu/Asp rich region
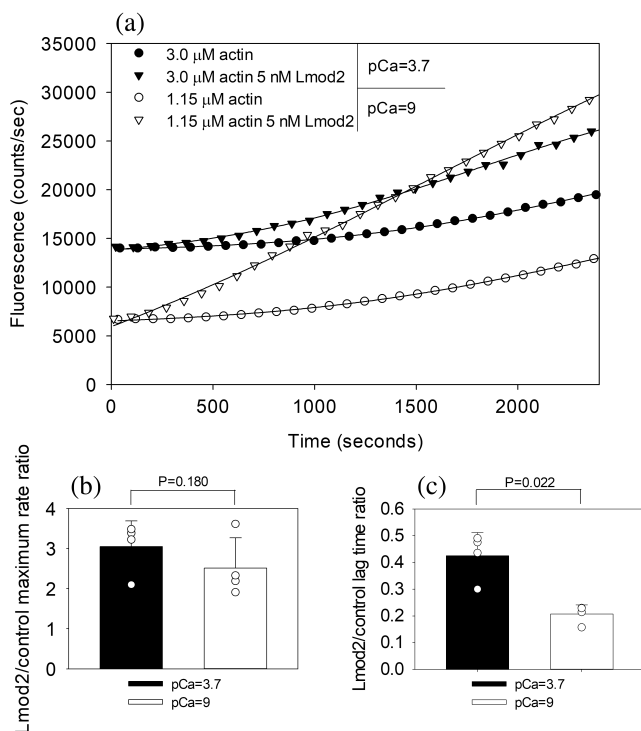
FIGURE 2 Effect of Ca^{2+} on Lmod2 nucleation observed by pyrene-actin polymerization assay. (a) Representative time courses of each condition with their sigmoidal fits shown by solid lines. (b) Lmod2/control maximum polymerization rate ratios. (c) Lmod2/control lag time ratios. Bars and error bars are the average and standard deviation, respectively. Values of each repeat are represented by circles, and the P-values were calculated by a paired t-test, $n = 4$

polymerization rates of G-actin in a range of concentrations from 1 to 2 μM at pCa = 9 (Figure S1). We found that 1.15 μM G-actin at pCa = 9 displays a similar rate of polymerization as 3.0 μM G-actin at pCa = 3.7. Therefore, these conditions were used to elucidate the effect of Ca^{2+} on Lmod2-induced actin nucleation (Figure 2a). Analysis of the polymerization curves revealed that at either pCa = 9 or pCa = 3.7, Lmod2 increased the maximum polymerization rate to the same extent (Figure 2b). At the same time, the lag time was differentially affected by adding Lmod2. It was reduced at pCa = 3.7 and pCa = 9 by a factor of ~2.5 and ~5, respectively (Figure 2c). This suggests that the presence of Ca^{2+} reduces the nucleation activity of Lmod2, since the lag phase of polymerization reflects the time required for the formation of actin nuclei.[21]

To confirm that the increase in pyrene fluorescence was due to the formation of actin filaments nucleated by Lmod2 we used TEM (Figure 3). The G-actin concentration was optimized for the TEM to keep the distribution of filaments on the carbon coated grids suitable for visualization. First, we compared polymerization of 2 μM G-

actin at Ca^{2+}-free (Figure 3a-c) and high Ca^{2+} (Figure 3d-f) conditions. Consistent with the pyrene-actin polymerization assay, at pCa = 9, G-actin polymerized faster than at pCa = 3.7, producing noticeably more filaments after 2 min of spontaneous polymerization (compare Figure 3b and e). However, very few actin filaments were found after 30 s of spontaneous polymerization at either Ca^{2+} level (Figure 3a and d). In contrast, addition of Lmod2 yielded short but well-organized actin filaments within the first 30 s (Figure 3g and j). The existence of those short filaments after such short times of polymerization is a hallmark of nucleation activity of Lmod2. Consistent with the pyrene-actin polymerization assay, the Ca^{2+}-free condition was more favorable for Lmod2-promoted actin polymerization, because, at pCa = 9 (Figure 3g), a larger number of short filaments were observed than at pCa = 3.7 (Figure 3j). The difference was even more noticeable after 2 min of incubation, since the Ca^{2+}-free condition yielded significantly denser population of actin filaments (compare Figure 3h and k). Therefore, our TEM data qualitatively confirmed the results obtained via the pyrene-actin polymerization assay: high Ca^{2+} levels inhibit Lmod2's potency to nucleate G-actin polymerization.

2.2 | Interaction of Lmod2 with cations

Attenuation of Lmod2's nucleation activity by Ca^{2+} implies that Ca^{2+} binds directly to Lmod2. There is an acidic region located within the 107-residue linker between the first two actin-binding sites of Lmod2 (Figure 1). Almost half of amino acid residues in this region are Glu and Asp residues. To study the putative Ca^{2+}-binding properties of Lmod2, we chose a fragment (Gly90-Tyr157) covering the acidic region. Hereafter we will refer to this fragment as EDRR (Glu(E)/Asp(D)-Rich Region).

We cloned and purified the fragment of Lmod2 representing EDRR. The fragment is a charged low complexity polypeptide, which makes it likely to be unstructured or poorly structured. With the exception of the well-structured ABS2 represented by the LRR domain,[22] Lmod2 is mostly disordered (Figure S2). Across all of the disorder predictors in the D^2P^2 database,[23] there is strong agreement that EDRR (Gly90-Tyr157) is a part of the disordered regions. To prove the disordered state of EDRR experimentally, we measured its circular dichroism (CD) spectrum (Figure S3). The shape of the spectrum was consistent with EDRR being a mostly disordered polypeptide, since the major minimum was at 197.5 nm. The helical content of EDRR calculated from the CD spectrum was only ~10%. Upon the addition of either
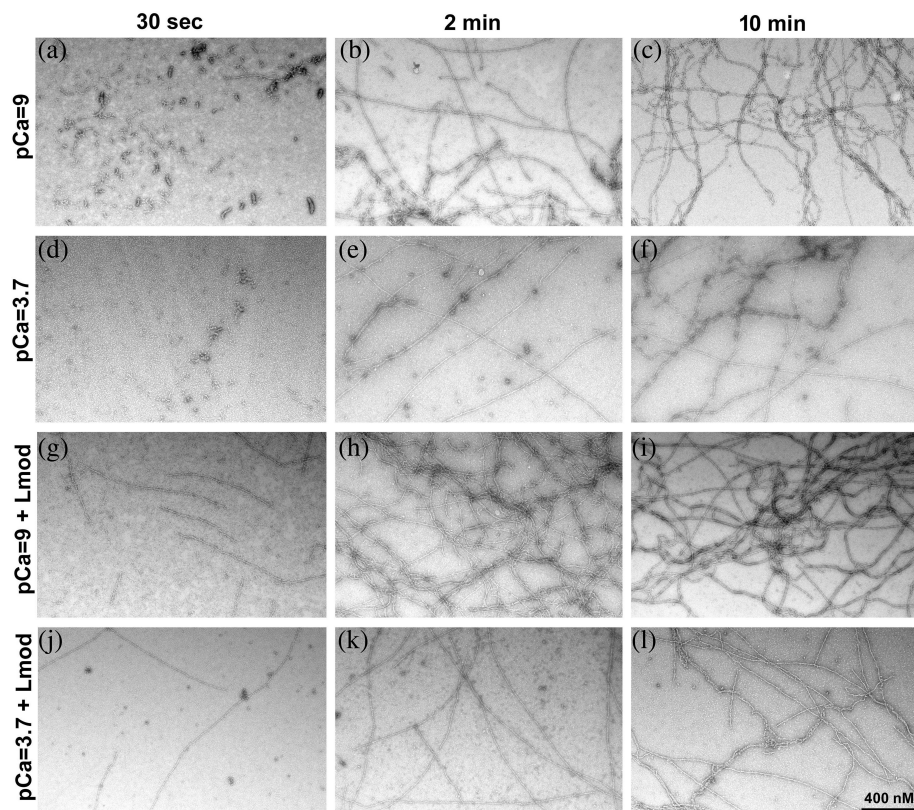
FIGURE 3 Spontaneous and Lmod2-nucleated polymerization of G-actin observed by electron microscopy of negatively stained samples at low and high Ca^{2+} levels. G-actin was polymerized in the absence (a-f) or presence (g-l) of 50 nM Lmod. Each trial was done at either low (a-c and g-i) or high (d-f and j-l) levels of Ca^{2+}, at 30 sec, 2 min and 10 min time points

Ca^{2+} or Mg^{2+}, at different cation to peptide ratios, we did not observe obvious changes in the shape of the EDRR CD spectrum (Figure S3), which suggests that neither cation causes a detectable change in the helical content. This is not unusual as cation binding is not always accompanied by a change in such secondary structure elements as α-helices and β-strands.[24–26]

To further evaluate the cation-binding ability of the EDRR fragment, we used NMR. Since the chemical shifts of nuclei are sensitive to their environment, the interaction of EDRR with cations could be detected as a change in the 1D proton NMR spectrum. Titrating the peptide with increasing concentrations of cations would not only allow us to conclude whether the observed changes in chemical shifts are distinct with respect to the chemical nature of the cation, but also whether they are dose-dependent. Therefore, we compared EDRR 1D proton NMR spectra using a range of either Ca^{2+} or Mg^{2+} concentrations (Figure 4).

The left (8.25–8.65 ppm) and the middle (7.95–8.35 ppm) panels in the titrations represent chemical shift ranges that primarily contain resonances belonging to backbone amide (NH) protons (Figure 4). In both Ca^{2+}- and Mg^{2+}-titrations, we observed similar changes in the amide proton spectra upon addition of either Ca^{2+} or Mg^{2+}. Therefore, 1D spectra of the region corresponding to the NH protons demonstrated that

EDRR binds Ca^{2+} and Mg^{2+}, but, judging by the changes in this spectral region alone, there was no indication that the binding is specific to a particular cation. Nevertheless, contrary to the similarity of the effect of Ca^{2+} and Mg^{2+} on the NH resonances, chemical shift changes of resonance peaks located in the side-chain region (represented by the right panels in the Figure 4, 2.5–3.2 ppm) were more pronounced upon the addition of Ca^{2+} rather than when Mg^{2+} was used. This observation suggested that the binding was specific with respect to the type of the cation used in titration. The response of the side-chain resonances to Ca^{2+} is indicative of a distinct secondary structure forming upon Ca^{2+} binding to EDRR.

2.3 | Effect of pre-incubation of Lmod2 with Ca^{2+} on Mg-actin nucleation

Despite the evidence that Ca^{2+} binds to the EDRR region of Lmod2, we could not completely eliminate the possibility that the observed effect of Ca^{2+} on the actin nucleation by Lmod2 arose from the effect of Ca^{2+} on the structure of the actin nucleus that might change the affinity of Lmod2 for G-actin. In the polymerization experiments presented above, we used G-actin with Ca^{2+} in its nucleotide-binding cleft. Upon adding Mg^{2+}-
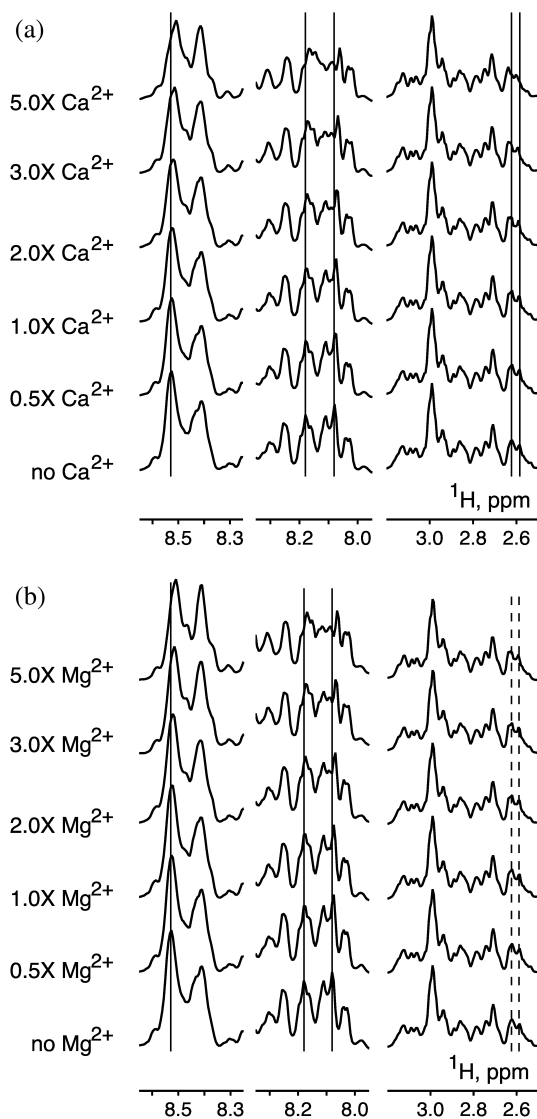
FIGURE 4   NMR titrations of the Lmod2 EDRR with Ca^{2+} and Mg^{2+}. Displayed are NMR spectral changes in three chemical shift regions upon addition of (a) Ca^{2+} and (b) Mg^{2+}. Molar excesses (0, 0.5, 1.0, 2.0, 3.0, and 5.0) of [cation] over [peptide] are shown to the left of the relevant spectra. Left and middle panels in both titrations (chemical shift regions 8.25–8.65 ppm and 7.95–8.35 ppm, respectively) correspond to resonance peaks of amide (backbone) protons. Right panels (chemical shift region 2.5–3.2 ppm) correspond to resonance peaks of side-chain protons. Solid vertical lines show initial (prior to cation addition) positions of the most affected peaks. Dashed vertical lines at ~2.6 ppm in (b) correspond to ~2.6 ppm solid lines in (a). The dashed lines demonstrate that side-chain-resonance peaks affected by Ca^{2+} are shifted markedly less when the peptide is titrated with Mg^{2+}

containing polymerization buffer, Ca^{2+} is expected to partially exchange with Mg^{2+}.[27] The rate of exchange depends on the $[Ca^{2+}]/[Mg^{2+}]$ ratio, and therefore, pCa = 9 and pCa = 3.7 conditions yield different

populations of Ca^{2+}- and Mg^{2+}-bound actin monomers. In such case, the indeterminate Ca/Mg-actin populations will introduce an uncertainty in our nucleation experiments.

To overcome this uncertainty, we exchanged the cation bound to actin from Ca^{2+} to Mg^{2+} prior to polymerization. We pre-incubated Lmod2 in a buffer containing Ca^{2+} to allow Ca^{2+} to bind to the protein. To choose the preferable Ca^{2+} concentration for the pre-incubation, we tested different Ca^{2+} concentrations in pyrene-actin polymerization assay in the absence of Lmod2 (Figure S4). Based on these experiments, we chose the Ca^{2+} concentration of 0.01 mM, which did not significantly affect the polymerization kinetics of Mg^{2+}-bound G-actin. Comparison of the actin nucleation and polymerization after addition of either Lmod2 or Lmod2 pre-incubated with Ca^{2+} revealed that the maximal rate of polymerization was not affected by pre-incubation with Ca^{2+}, while the lag time was noticeably increased (Figure 5). Therefore, our data suggested that the effect of Ca^{2+} on Lmod-induced nucleation was primarily due to Ca^{2+} binding to Lmod2.

3 | DISCUSSION

Striated muscles rely on a Ca^{2+} transient for the contraction mechanism to proceed, and the Ca^{2+} transient affects the properties/functions of many essential muscle proteins, for example, troponin, myosin, titin, and myosin-binding protein C.[1,3–5] However, the effect of Ca^{2+} on the activity of the members of the Tmod family proteins has never been examined.

In this study, we demonstrated that Ca^{2+} affects Lmod2 nucleation ability most likely by binding to the acidic region. The acidic region is present in the ABS1-ABS2 linker of the striated muscle isoforms, Lmod2 and Lmod3, but it is absent in Lmod1, the smooth muscle isoform.[19] In Lmod2, this region displays a large degree of homology across species (Figure S5), which suggests that it performs an important cellular function.

With respect to Lmod2 molecular interactions, most previous research efforts have been focused on the structure of interfaces between Lmod consensus binding sites (Figure 1) and Tpm or actin.[9,22,28–31] Much less attention has been paid to the linkers connecting the actin-binding domains; thus, their functional significance has been unknown. Based on its sequence, it has been suggested that the ABS1-ABS2 linker should be disordered,[9] and the disorder prediction confirms this (Figure S2). The ABS1-ABS2 linker does not bind Tpm,[29] and it has been shown that a region between Glu124 and Gly201 within the linker might interact with actin.[29]
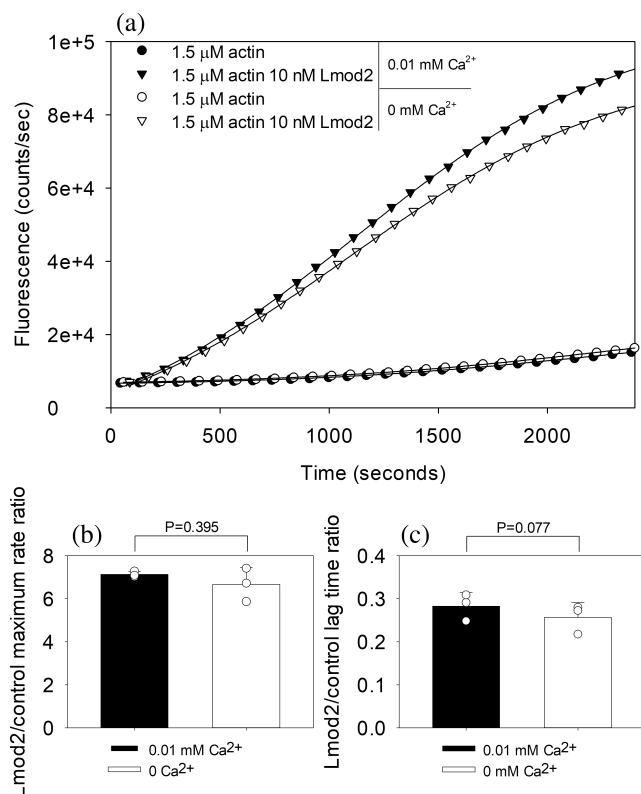
FIGURE 5 Effect of pre-incubation of Lmod2 with Ca^{2+} on nucleation of Mg-actin observed by pyrene-actin polymerization assay. (a) Representative time courses of each condition with sigmoidal fits represented by solid lines. (b) Lmod2/control maximum polymerization rate ratios. (c) Lmod2/control lag time ratios. Values of each repeat are represented by circles, and the P-values were calculated by a paired *t*-test, $n = 4$

Clearly, Ca^{2+} affects the ability of Lmod2 to nucleate actin (Figures 2 and 5). The search for a consensus Ca-binding motif (e.g., an EF hand motif found in TnC[4] and myosin light chains[5]) did not give us any matches in Lmod2. Therefore, our data suggest that the ABS1-ABS2 linker harbors a unique Ca^{2+}-binding site. It might be similar to the so-called condensed-charge motif that has been shown to bind Ca^{2+}, among other divalent cations, in proteins, such as starmaker, α-synuclein, and prothymosin α.[25] In proteins, Ca^{2+} is typically coordinated by side-chain oxygen atoms of Asp, Glu, and Asn.[32] In addition to 29 Glu and 4 Asp, there are 2 Asn residues located within the acidic region (Figure S5). Since the coordination geometry of Ca^{2+} is usually octahedral, we can estimate that 3–6 residues are required to form the complete coordination sphere. Based on the total number of residues Asp, Glu, and Asn alone, the EDRR can potentially bind up to 6–12 Ca^{2+} cations; however, considering the coordination geometry requirements, this number is likely to be smaller. Moreover, only a few of these residues may be responsible for the specific Ca^{2+}

binding that affects Lmod2 function. Further studies are necessary to determine residues that are responsible for the specific Ca^{2+} binding.

The geometric requirements should also reduce the number of conformations that the mostly disordered ABS1-ABS2 linker containing the EDRR can adopt. As a result, an average end-to-end distance of the linker might be reduced upon binding Ca^{2+}. This could make the formation of nuclei by ABS1 and ABS2 binding to actin monomers less favorable, manifesting itself as a reduction in the nucleation activity of Lmod2 when it is Ca^{2+}-bound. Indeed, the cooperation between ABS1 and ABS2 is important for Lmod2 nucleation.[13]

The present study calls for further investigation into the connection between the apparent Ca^{2+} sensitivity of Lmods and the role of Lmods in thin filament maintenance. It is possible that for Lmod to promote the formation of new thin filaments, it should happen when the muscle is relaxed and the free Ca^{2+} is low. Further characterization of the Ca^{2+} sensitivity of Lmods could change our understanding of the thin filament length regulation mechanism in striated muscles.

4 | MATERIALS AND METHODS

4.1 | Cloning of the recombinant Lmod2 Glu/asp-rich region EDRR

The amino acid sequence of mouse Lmod2 (NP_444328.1) was from the National Center for Biotechnology Information (Bethesda, MD). DNA primers for cloning were from Integrated DNA Technologies (Coralville, IA). Restriction enzymes XhoI and EcoRI, OneTaq DNA polymerase, T4 ligase, and relevant buffers and solutions were supplied by New England Biolabs (Ipswich, MA). Synthesis of template DNA optimized for *Escherichia coli* expression[33] was performed by GenScript Biotech (Piscataway, NJ). The DNA sequence encoding residues Gly90-Tyr157 of the mouse Lmod2 was cloned as an MFH-fusion protein by following the protocol of cloning Tmod2-TpmBS2 described previously.[34] To facilitate the fragment production and spectral data collection, Cys118 was replaced with Tyr, which is a highly conservative residue in mammalian Lmod2. Generation of a mutagenized expression vector incorporating the C118Y substitution was performed as we did before[9] using two partially overlapping primers 5′-GGAAGTT-**TAC**-ACGGAAGATGAAGAGGAATCTCAGGAAGAAGA-3′ and 5'-CTTCCGT-**GTA**-AACTTCCTCCGATACCTCG GAATTAGATTCAG-3′. In the primers, complementary codons encoding Tyr118 are shown in bold. DNA

sequences of the recombinant constructs were confirmed by Sanger sequencing (performed at GeneWiz, South Plainfield, NJ).

4.2 | EDRR expression and purification

Expression in LB medium and purification of the MFH-fusion protein were performed following the same protocols that we used for other MFH-fused constructs.[28] The eluted from Ni-NTA fusion protein was dialyzed against 5 mM HCl with 2 dialysis solution changes, brought to 0.2 M in HCl, and cleaved overnight with a 400-fold molar excess of CNBr. The reaction mixture was applied onto a Sep-Pak C18 cartridge from Waters (Milford, MA) and washed with six bed volumes of 0.1% trifluoroacetic acid (TFA). The MFH tag and the uncleaved MFH-fusion protein were removed from the column with 60% acetonitrile in 0.1% TFA. The Lmod2 EDRR was eluted from the Sep-Pak column with a mixture of acetonitrile and 1% ammonium bicarbonate (6:4 vol:vol), dialyzed against 5 mM HCl and lyophilized. Concentration of the peptide was determined by measuring its extinction at 280 nm and comparing it with the molar peptide extinction predicted by an online ProtParam Expasy tool[35] or using the difference in spectra in 6 M GuHCl between pH 12.5 and pH 7.0 as described in.[36]

4.3 | Protein purification

The G-actin was purified according to protocols in,[29] with some modifications. Reconstituted F-actin pellets, after polymerization and removal of Tpm and TnT, were combined and sonicated in a bath sonicator on ice for 30 min. After dialysis to depolymerize actin, the solution was sonicated with a probe sonicator for 2 min then centrifuged at 80,000 rpm (rotor MLA-80) and 4°C for 2 h and 10 min. G-actin in the supernatant was purified on a Sephacryl S-300 gel filtration column equilibrated with Buffer A. The P-actin was prepared and purified according to protocols in.[29] Lmod2 was expressed and purified as previously described.[37] All protein concentrations were determined by measuring the difference in spectra in 6 M GuHCl between pH 12.5 and pH 7.0.[36]

4.4 | Nuclear magnetic resonance titration

The NMR samples were prepared in 20 mM HEPES-d$_{18}$ (pH 6.8), which was obtained from the Cambridge

Isotope Laboratories (Tewksbury, MA). The samples contained 10% D$_2$O and 0.2 mM DSS, both purchased from the Cambridge Isotope Laboratories. The concentration of the Lmod2 EDRR was 0.3 mM. The sample was titrated with small aliquots of 10 mM and 30 mM CaCl$_2$ or MgCl$_2$ stock solutions (adjusted to pH ~6.8). 1H NMR spectra were recorded at 25°C on a Varian Inova 500 spectrometer (500 MHz) equipped with a 5 mm triple-resonance probe. The spectra were processed, visualized, and analyzed with Mnova (Mestrelab Research, Santiago de Compostela, Spain).

4.5 | Circular dichroism

CD measurements were taken using an Aviv model 420 spectropolarimeter (Lakewood, NJ). The spectrum of 6 μM EDRR in 10 mM HEPES, pH 7.0, containing 100 mM NaCl was recorded in a 1 mm cuvette at 10°C. Helical content was calculated as in.[38] Disordered regions in Lmod2 were predicted using the Database of Disordered Protein Predictions (D^{2}P^2) at https://d2p2. pro/.[23]

4.6 | Fluorescence measurement of Lmod2 nucleation at pCa = 3.7 and pCa = 9

Actin polymerization was measured as the change in fluorescence of pyrene-actin on a PTI fluorometer (10 mm cuvette, 366 nm excitation, 387 nm emission, and 2 nm slit). Pyrene-actin was added to 10% of the actin concentration. To measure the effect of Ca^{2+} on actin polymerization and Lmod2 nucleation of actin, aliquots of concentrated 20X polymerization buffer with or without 20X CaCl$_2$ were added to initiate polymerization at room temperature. The final compositions of the polymerization buffers in the polymerization mixtures were: 100 mM KCl, 2 mM MgCl$_2$, 2 mM EGTA, 1 mM DTT, 0.1 mM ATP, 25 mM imidazole pH 8.0, with (pCa 3.7) or without (pCa 9) 2 mM CaCl$_2$. For our experiments, pCa ($pCa = -\log[Ca^{2+}]$, where $[Ca^{2+}]$ is free Ca^{2+} concentration) was calculated by using a web-based pCa calculator called CHELATOR.[39] The calculation was based on the buffer contents and the ionic strength, and the ionic strength was calculated using Ionic Strength Calculator http://calistry.org/calculate/ionic-strength-calculator. We first polymerized 3.0 μM G-actin at pCa = 3.7 and 1.0 μM, 1.15 μM, 1.5 μM, and 2.0 μM G-actin at pCa = 9 (Figure S1). The maximum polymerization rates of 3.0 μM at pCa 3.7 and 1.15 μM actin at pCa = 9 were ~4.2 and ~4.5 respectively (Figure S1). So we chose to continue with 3.0 μM actin at pCa = 3.7 and 1.15 μM

actin at pCa = 9 to elucidate the effects of Ca^{2+} on Lmod2-indiuced nucleation; 5 nM Lmod2 was added right before adding polymerization buffer with or without $CaCl_2$. Polymerization of actin in the absence of Lmod2 was measured as a control. The curves were fitted to a four-parameter sigmoid function in SigmaPlot 12, the rate of polymerization was calculated as the first derivative of the function, and a tangent line to the point of the maximum rate was plotted. The lag time for actin polymerization was calculated by finding the intersection between the tangent line and the minimum fluorescence value (y-value) of the curve as in.[21]

4.7 | Polymerization of Mg-actin with Lmod2 pre-incubated with Ca^{2+}

At pCa = 9, in the presence of 1 nM Ca^{2+} and 2 mM Mg^{2+}, Ca-actin is converted to Mg-actin with $t_{1/2} \sim 40$ sec, according to the competitive exchange model.[27] At pCa = 3.7, in the presence of 0.2 mM Ca^{2+}, 2 mM $MgCl_2$, and 2 mM $CaCl_2$, Ca-actin is converted to Mg-actin with $t_{1/2} \sim 450$ sec. In each condition, there is a different population of Ca^{2+} or Mg^{2+} bound actin over time. Exchanging the actin-bound cation to Mg^{2+} before performing nucleation experiments largely averts this problem. To exchange the Ca-actin to Mg-actin, pyrene-actin was first added to 10% of the actin concentration, then incubated in 0.05 mM EGTA and 0.05 mM $MgCl_2$ at room temperature for 6 min as in.[20] The actin was then applied to and eluted from a Cytiva PD-10 MiniTrap desalting column packed with Sephadex G-25 resin using an actin buffer containing 2 mM Tris–HCl pH 8.0, 0.05 mM $MgCl_2$, 0.01% NaN_3, 0.5 mM DTT, and 0.2 mM ATP. Concentrated 20X polymerization buffer was added to allow polymerization to begin at room temperature. The final composition of the polymerization buffer in the polymerization mixtures was: 150 mM KCl, 0.1 mM $MgCl_2$, 1 mM DTT, 0.1 mM ATP, 25 mM imidazole, pH 8.0. We first polymerized 1.5 μM Mg-actin in increasing concentrations of Ca^{2+}, from 0 to 0.05 mM (Figure S2A). We chose 0.01 mM Ca^{2+} based on the observation that higher Ca^{2+} concentrations affect the polymerization of Mg-actin (Figure S2B). To prepare working solutions of Lmod2, we diluted a 12.8 μM Lmod2 stock to 0.5 μM, with or without 0.5 mM Ca^{2+}. After at least 10 min of incubation time, Lmod2 with or without Ca^{2+} was added right before adding polymerization buffer, to make the final concentrations

10 nM Lmod2 and 0.01 mM Ca^{2+}. The curves were analyzed as before.

4.8 | Transmission electron microscopy

Two μM G-actin was polymerized at room temperature using the same conditions as described for fluorescent measurements. Aliquots of the polymerizing actin were used for negative staining at 30 s, 2 min, and 10 min time points. A small volume (7 μL) of each sample was incubated for 30 s on carbon-coated, glow-discharged grid (Electron Microscopy Sciences, FCF300-Cu-SB) and blotted with filter paper. After negative staining with 2% (w/v) uranyl acetate, grids were analyzed using JEM-1200EX (JEOL) Transmission Electron Microscope at an accelerating voltage of 70 kV to record micrographs at a nominal magnification of 30,000×.

ORCID

Garry E. Smith https://orcid.org/0000-0001-9544-0938

Dmitri Tolkatchev https://orcid.org/0000-0002-1300-6458

Alla S. Kostyukova https://orcid.org/0000-0002-6724-2069

REFERENCES

1. DuVall MM, Gifford JL, Amrein M, Herzog W. Altered mechanical properties of titin immunoglobulin domain 27 in the presence of calcium. Eur Biophys J. 2013;42:301–307.
2. Kuhn ER, Naik AR, Lewis BE, et al. Nanothermometry reveals calcium-induced remodeling of myosin. Nano Lett. 2018;18:7021–7029.
3. Previs MJ, Mun JY, Michalek AJ, et al. Phosphorylation and calcium antagonistically tune myosin-binding protein C's structure and function. Proc Natl Acad Sci U S A. 2016;113:3239–3244.
4. Marston S, Zamora JE. Troponin structure and function: A view of recent progress. J Muscle Res Cell Motil. 2020;41:71–89.
5. Heissler SM, Sellers JR. Myosin light chains: Teaching old dogs new tricks. Bioarchitecture. 2014;4:169–188.
6. Tolkatchev D, Gregorio CC, Kostyukova AS. The role of leiomodin in Actin dynamics: A new road or a secret gate. FEBS J. 2021;16128.
7. Prill K, Dawson JF. Assembly and maintenance of sarcomere thin filaments and associated diseases. IJMS. 2020;21:542.
8. Weber A, Pennise CR, Babcock GG, Fowler VM. Tropomodulin caps the pointed ends of Actin filaments. J Cell Biol. 1994;127:1627–1635.
9. Tolkatchev D, Smith GE Jr, Schultz LE, et al. Leiomodin creates a leaky cap at the pointed end of Actin-thin filaments. PLoS Biol. 2020;18:e3000848.
10. Kostyukova AS, Choy A, Rapp BA. Tropomodulin binds two tropomyosins: A novel model for Actin filament capping. Biochemistry. 2006;45:12068–12075.
11. Rao JN, Madasu Y, Dominguez R. Mechanism of Actin filament pointed-end capping by tropomodulin. Science. 2014;345:463–467.
12. Tsukada T, Pappas CT, Moroz N, Antin PB, Kostyukova AS, Gregorio CC. Leiomodin-2 is an antagonist of tropomodulin-1 at the pointed end of the thin filaments in cardiac muscle. J Cell Sci. 2010;123:3136–3145.
13. Boczkowska M, Rebowski G, Kremneva E, Lappalainen P, Dominguez R. How Leiomodin and Tropomodulin use a common fold for different Actin assembly functions. Nat Commun. 2015;6:8314.
14. Chereau D, Boczkowska M, Skwarek-Maruszewska A, et al. Leiomodin is an Actin filament nucleator in muscle cells. Science. 2008;320:239–243.
15. Pappas CT, Mayfield RM, Henderson C, et al. Knockout of Lmod2 results in shorter thin filaments followed by dilated cardiomyopathy and juvenile lethality. Proc Natl Acad Sci U S A. 2015;112:13573–13578.
16. Yuen M, Sandaradura SA, Dowling JJ, et al. Leiomodin-3 dysfunction results in thin filament disorganization and nemaline myopathy. J Clin Invest. 2014;124:4693–4708.
17. Halim D, Wilson MP, Oliver D, et al. Loss of LMOD1 impairs smooth muscle cytocontractility and causes megacystis microcolon intestinal hypoperistalsis syndrome in humans and mice. Proc Natl Acad Sci U S A. 2017;114:E2739−E2747.
18. Cenik BK, Garg A, McAnally JR, et al. Severe myopathy in mice lacking the MEF2/SRF-dependent gene leiomodin-3. J Clin Invest. 2015;125:1569–1578.
19. Fowler VM, Dominguez R. Tropomodulins and Leiomodins: Actin pointed end caps and Nucleators in muscles. Biophys J. 2017;112:1742–1760.
20. Selden LA, Estes JE, Gershman LC. The tightly bound divalent cation regulates Actin polymerization. Biochem Biophys Res Commun. 1983;116:478–485.
21. Nishida E, Sakai H. Kinetic analysis of Actin Polymerization1. The Journal of Biochemistry. 1983;93:1011–1020.
22. Boczkowska M, Yurtsever Z, Rebowski G, Eck MJ, Dominguez R. Crystal structure of Leiomodin 2 in complex with Actin: A structural and functional reexamination. Biophys J. 2017;113:889–899.
23. Oates ME, Romero P, Ishida T, et al. D2P2: Database of disordered protein predictions. Nucleic Acids Res. 2012;41:D508–D516.
24. Uversky VN, Gillespie JR, Millett IS, et al. Zn2+−mediated structure formation and compaction of the "natively unfolded" human Prothymosin α. Biochem Biophys Res Commun. 2000;267:663–668.
25. Newcombe EA, Fernandes CB, Lundsgaard JE, et al. Insight into calcium-binding motifs of intrinsically disordered proteins. Biomolecules. 2021;11:1173.
26. Chichkova NV, Evstafieva AG, Lyakhov IG, et al. Divalent metal cation binding properties of human prothymosin α: Zn2+,Ca2+−binding by prothymosin α. Eur J Biochem. 2000;267:4745–4752.
27. Gershman LC, Selden LA, Estes JE. High affinity divalent cation exchange on Actin. Association rate measurements support the simple competitive model. J Biol Chem. 1991;266:76–82.
28. Colpan M, Tolkatchev D, Grover S, et al. Localization of the binding interface between leiomodin-2 and alpha-tropomyosin. Biochim Biophys Acta. 2016;1864:523–530.
29. Ly T, Moroz N, Pappas CT, et al. The N-terminal tropomyosin- and Actin-binding sites are important for leiomodin 2's function. Mol Biol Cell. 2016;27:2565–2575.
30. Kostyukova AS. Leiomodin/tropomyosin interactions are isoform specific. Arch Biochem Biophys. 2007;465:227–230.
31. Arslan B, Colpan M, Gray KT, Abu-Lail NI, Kostyukova AS. Characterizing interaction forces between Actin and proteins of the tropomodulin family reveals the presence of the N-terminal Actin-binding site in leiomodin. Arch Biochem Biophys. 2018;638:18–26.
32. Zheng H, Chruszcz M, Lasota P, Lebioda L, Minor W. Data mining of metal ion environments present in protein structures. J Inorg Biochem. 2008;102:1765–1776.
33. Puigbo P, Guzman E, Romeu A, Garcia-Vallve S. OPTIMIZER: A web server for optimizing the codon usage of DNA sequences. Nucleic Acids Res. 2007;35:W126–W131.
34. Tolkatchev D, Kuruba B, Smith GE Jr, et al. Structural insights into the tropomodulin assembly at the pointed ends of Actin filaments. Protein Sci. 2020;30:423–437.

35. Wilkins MR, Gasteiger E, Bairoch A, et al. Protein identification and analysis tools in the ExPASY server. In: Link AJ, editor. In 2D proteome analysis protocols, volume 112, methods in molecular. Biology ed. Humana Press, Totowa, NJ; 1999.

36. Kostyukova AS, Hitchcock-Degregori SE, Greenfield NJ. Molecular basis of tropomyosin binding to tropomodulin, an Actin-capping protein. J Mol Biol. 2007;372:608–618.

37. Ly T, Pappas CT, Johnson D, et al. Effects of cardiomyopathy-linked mutations K15N and R21H in tropomyosin on thin-filament regulation and pointed-end dynamics. Mol Biol Cell. 2019;30:268–281.

38. Greenfield NJ. Using circular dichroism spectra to estimate protein secondary structure. Nat Protoc. 2006;1:2876–2890.

39. Schoenmakers TJ, Visser GJ, Flik G, Theuvenet AP. CHELA-TOR: An improved method for computing metal ion concentrations in physiological solutions. Biotechniques. 1992;12(870–874):876–879.

SUPPORTING INFORMATION

Additional supporting information can be found online in the Supporting Information section at the end of this article.